Pergamon

Deep-Sea Research I, Vol. 44, No. 11, pp. 1739–1767, 1997

0967–0637/98 $19.00 + 0.00

PII: S0967–0637(97)00029–0

Particle size spectra between 1 μm and 1 cm at Monterey Bay determined using multiple instruments

GEORGE A. JACKSON,* ROBERT MAFFIONE,† DAVID K. COSTELLO,‡ ALICE L. ALLDREDGE,§ BRUCE E. LOGAN¶ and HANS G. DAM‖

(*Received* 19 *April* 1996; *accepted* 23 *October* 1996)

Abstract—Particles are responsible for the vertical transport of material in the ocean. Size is an important characteristic of a particle, determining its fall velocity, mass content, scattering cross-section, and food value, as well as other properties. The particle size spectrum describes the distribution of particles in a volume of water as a function of their sizes. We measured particle size spectra in Monterey Bay, CA, using six different instruments that examined particles ranging from approximately 1 μm to 10 mm. Before the results could be combined, they had to be adjusted for the different particle properties actually measured. Results from different optical instruments were similar, although the spectral values were sensitive to minor variations in the diameter assigned to particles. Sample volume was crucial in determining the effective upper size limit for the different techniques. We used fractal scaling to piece the results together, deriving fractal dimensions of 2.26–2.36. Diver observations of visible particles showed that they were composed mostly of aggregated diatoms. The particle size spectra n_I were remarkably well fitted with a power law function $n_I = ad_I^{-b_I}$, where d_I is the image diameter and $b_I = 2.96$–3.00. The equivalent slopes for particles measured with an aperture impedance instrument were 3.50–3.61. The particle volume distribution showed that most of the particle mass was in the 0.1–3 mm range. This volume distribution is consistent with theories that assume particle sizes are controlled by simultaneous coagulation and disaggregation. © 1998 Elsevier Science Ltd.

INTRODUCTION

Ranging from the almost dissolved colloids about 1 nm in size to organisms many meters long, particles are concentrated packets of material in a dilute ocean. By active swimming or passive settling, particles work against homogenization by a turbulent ocean, moving matter from one region to another. As small particles collide and combine to form larger particles, the physical processes that affect them change from molecular diffusion to turbulent shear, settling and swimming. The importance of size in controlling their interactions with the environment makes an accurate description of particle size distributions an essential part of understanding particles and their role in modifying the environment.

* Department of Oceanography, Texas A&M University, College Station, TX 77843, USA.
† Hydro-Optics, Biology, and Instrument Laboratories, 55 Penny Lane, Watsonville, CA 95076, USA.
‡ Marine Science Department, University of South Florida, St. Petersburg, FL 33701, USA.
§ Marine Sciences Institute, University of California, Santa Barbara, Santa Barbara, CA 93106, USA.
¶ Department of Civil and Environmental Engineering, The Pennsylvania State University, University Park, PA 16802, USA.
‖ Department of Marine Sciences, University of Connecticut, Groton, CT 06340, USA.

One description of particle concentration and size distribution is the cumulative particle size distribution N, where $N(s)$ is the number of particles per unit volume greater than a size s (see Table 1 for notation). The particle size can be volume, surface area, cross-sectional area, diameter, radius or any other measure of how big a particle is. More useful is the related particle size spectrum n, the concentration of particles per unit size interval. It is also known as the differential size spectrum to distinguish it from N. The two descriptors of particle distributions are related by

$$n(s) = -\frac{dN}{ds} \tag{1}$$

Table 1. *Notation*

Symbol	Definition	Units
a	Constant describing spectrum	
b	Constant describing spectrum	
B	Constant	
c	Constant for fractal scaling	
c_1, c_2, c_3, and c_4	Constants	
C	Carbon content of cell	pg-C cell^{-1}
d	Particle diameter	cm
d_0	Diameter of monomer	cm
d_c	Conserved diameter	cm
d_g	Diameter of gyration ($=2r_g$)	cm
d_I	Image diameter	
d_x	Diameter at which n_I and n_c are equal	
D	Fractal dimension	
m_k	Mass of kth subparticle in aggregate	
M	Total aggregate mass	
n	Particle size spectrum	cm^{-4}
n_c	Particle size spectrum for d_c	
$n_{c,j}$	n_c interpolated to jth point	
n_I	Particle size spectrum for d_I	
$n_{I,j}$	n_I transformed to d_c equivalents for jth value	
n_{min}	Minimum n calculable	cm^{-4}
N	Cumulative particle size distribution	cm^{-3}
P_C	Particulate organic carbon concentration	
r_0	Radius of monomer	cm
r_g	Radius of gyration (r.m.s. radius)	cm
r_k	Distance from aggregate center to kth subparticle	
s	Generic particle size	arbitrary
s_l	Lower bound of a size range	
s_u	Upper bound of a size range	
V	Volume of cell	μm^3
V_c	Conserved particle volume	cm^3
V_{samp}	Volume sampled	
V_{TC}	Total conserved particle volume from POC	
V_{TS}	Total conserved particle volume for spectrum	
α	Constant	
γ	Constant relating d_x to d_0	
λ	Constant	
ρ_c	Constant to convert POC to volume	
σ	Fitting error	

The property n is usually estimated by counting the number of particles within a given size range and dividing that number by the extent of the size range and the volume sampled. Because the value of n is estimated using whole number counts, the minimum particle size spectrum that can be measured $n_{\min}(s)$ occurs when there is one particle in a size range:

$$n_{\min}(s) = \frac{1 \text{ particle}}{(s_u - s_l) \cdot V_{\text{samp}}} \tag{2}$$

where s_u and s_l are the upper and lower values of the size range and V_{samp} is the volume of water being sampled.

Equation (1) can be used to relate size spectra expressed in terms of different measures of particle size. For example, a spectrum $n(d)$ expressing size in terms of particle diameter d is related to $n(V_c)$, the spectrum in terms of conserved, or solid, volume by

$$n(V_c) = n(d)\frac{dd}{dV_c} \tag{3}$$

Segments of the particle size spectrum often fit an expression of the form

$$n(d) = ad^{-b} \tag{4}$$

where a and b are constants and d is the particle diameter (e.g. Sheldon *et al.*, 1972; Lal, 1977). The value of b has been used to infer information about the processes forming the aggregates (e.g. Friedlander, 1977; Hunt, 1980a, 1982). Most such work in aquatic systems has been done for relatively narrow size ranges, typically 1–100 μm (e.g. McCave, 1983, 1984; Eisma, 1986; Sternberg *et al.*, 1988).

For aggregates, the relationship between particle diameter and particle volume is complicated by the fact that aggregates are porous objects, with a porosity that increases with aggregate diameter. This variable porosity results in apparent sizes for particles that are not related to the particle mass in the same way that the diameter of a solid sphere is related to its volume and mass. Measures of apparent particle size could include the diameter of the smallest sphere capable of encasing the particle, the square root of the projected area, and the r.m.s. radius, also known as the radius of gyration r_g. These measures of apparent particle radius and diameter are linearly related to each other for particles formed by aggregation processes because they exhibit what is known as fractal scaling (e.g. Rogak and Flagan, 1990; Logan and Kilps, 1995). The relationship between particle length and conserved volume (the volume of the solid constituents of an aggregate, which is proportional to the solid mass when the matter is of constant density) for such fractal scaling is

$$V_c = cd_g^D \tag{5}$$

where D is the fractal dimension, the diameter of gyration is defined as $d_g = 2r_g$, and c is a constant (e.g. Avnir, 1989; Vicsek, 1992). If an aggregate is composed of p sub-particles of mass m_k located a distance r_k from the aggregate's center of mass, then

$$r_g = \left(M^{-1} \sum_{k=1}^{p} m_k r_k^2 \right)^{0.5} \tag{6}$$

where $M = \sum_{k=1}^{p} m_k$ is the total aggregate mass (e.g. Jackson and Lochmann, 1993). If the

sub-particles are all the same, as would be expected for an initially mono-disperse system, then this reduces to

$$r_g = \left(p^{-1} \sum_{k=1}^{p} r_k^2 \right)^{0.5}. \tag{7}$$

For a solid sphere of radius r_0, r_g is determined by integration:

$$\begin{aligned} r_g &= \left[\left(\frac{4\pi}{3} r_0^3 \right)^{-1} \int_0^{r_0} r^2 \cdot 4\pi r^2 \, dr \right]^{0.5} \\ &= \left(\frac{3}{5} \right)^{0.5} r_0. \end{aligned} \tag{8}$$

The values of c and D depend on the system. If the aggregates are not porous, D is three. Values of D have been estimated for marine systems that range from 1.26 to 2.49 (e.g. Logan and Wilkinson, 1990; Li and Logan, 1995; Jackson *et al.*, 1995). Smaller values of D usually indicate more porous structures.

The fractal properties of particles are important when particle size spectra obtained with different instruments are compared, because the instruments measure different particle properties. For example, aperture impedance particle counters, such as the Coulter and the Elzone particle counters, measure a property that approximately, but not exactly, corresponds to the volume of the solid particles composing an aggregate. Imaging systems usually measure the cross-sectional area of the porous aggregate, which is then used to calculate the image diameter d_i. Jackson *et al.* (1995) used equations (3) and (5) to combine imaging and aperture impedance spectra in a marine mesocosm of aggregating algae. In this, they were using the fact that the length obtained from the projected area of a fractal structure is proportional to d_g (e.g. Logan and Kilps, 1995).

Although equation (5) suggests a way to calculate c and D by comparing particle mass and the diameter of gyration, this is true only when measurements of both properties exist on the same particles. Attempts to use measurements from different instruments that are measuring over different size ranges are more problematic.

This paper describes particle size spectra over a range of almost $1–10^4$ μm measured off California. Because constructing these spectra required combining results from different instruments, we examine the data from the different instruments before combining them.

SAMPLE SITE

Data were taken as part of a program to study particle size spectra in Monterey Bay funded by the Office of Naval Research (ONR). Data discussed here were collected on 29 July 1993, in 70 m of water at 36°50′ N, 121°53′ W. The operation used two vessels (R.V. *Sproul* and R.V. *Shana Rae*) to allow relatively synchronous data collection. Water samples for analysis by laboratory instrumentation were collected using 30 l Niskin bottles. *In situ* instruments were deployed as soon as possible thereafter from both vessels. All samples were collected within 1 h of each other, at around 11:00 h Pacific Daylight Time. The samples discussed here were collected at nominal depths of 10, 15, and 30 m. Although information exists on particle spectra at other depths, these three depths represent regions where all the instruments sampled.

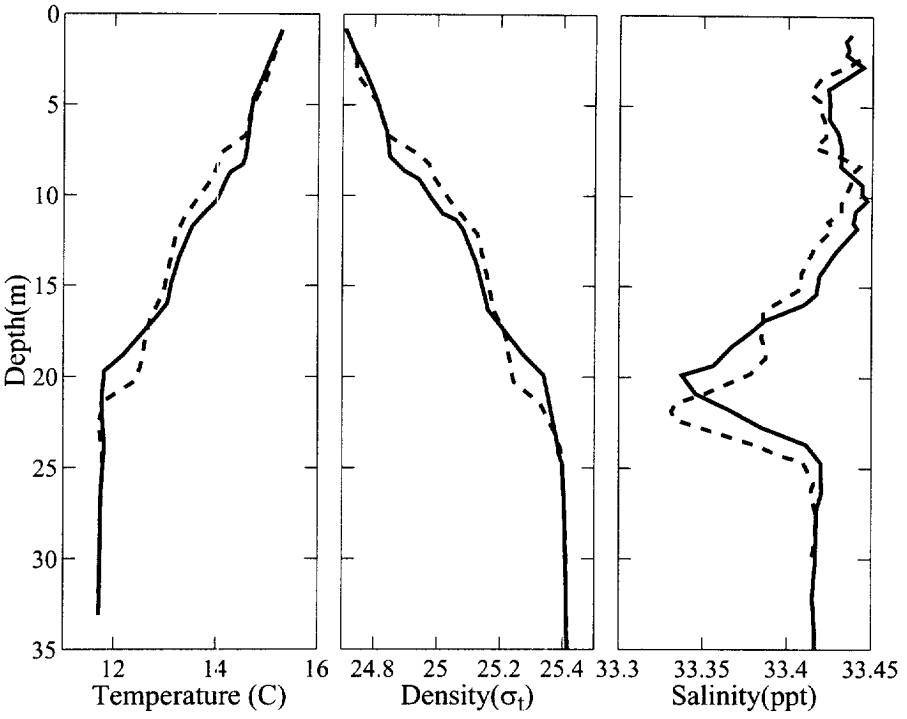

Fig. 1. Vertical water column structure at 10:50 h, 29 July 1993. Left: temperature; center: density; right: salinity. Nitrate concentrations were 2.5, 5, 9.4, and 16.2 μM at 3 m, 5 m, 15 m, and 30 m, respectively.

Monterey Bay is the site of intense upwelling of water with high nutrient concentrations (e.g. Graham, 1993). High phytoplankton concentrations and aggregates formed from algae have been observed there (Trent *et al.*, 1978). The physical properties of the water column during our program indicate the water had a strong temperature and density gradient from the surface to about 20 m, with a substantially weaker gradient deeper (Fig. 1). Observations over time indicate that the water profile was very active, with internal waves causing strong vertical shifts in isopycnals. There was also a tongue of low salinity water (33.35‰) in the midst of the higher salinity water column (33.40–33.45‰). Nutrient concentrations in the region were high, with nitrate concentrations being 2.5 μM, 5.0 μM, 9.4 μM, and 16.2 μM at 3 m, 10 m, 15 m and 30 m, respectively.

The particle concentrations as measured by the dry weight concentration were relatively constant through the water column at about 4 mg l^{-1} (Fig. 2). Particulate organic carbon (POC) concentrations did change with depth, decreasing from 0.26 mg l^{-1} at 7 m to 0.14 mg l^{-1} at 30 m (Fig. 2). Methods for sample collection and analyses have been described by Alldredge *et al.* (1995). Divers reported that the water between 0 and 14 m was very green, with extensive suspended material that, upon collection and examination, was composed of diatoms of approximately 10 μm length of the genus *Thalassiosira*. Aggregates collected between 14 and 25 m were composed of large *Chaetoceros peruvianus* or *C. concavicornis* cells with ciliates and some fecal material.

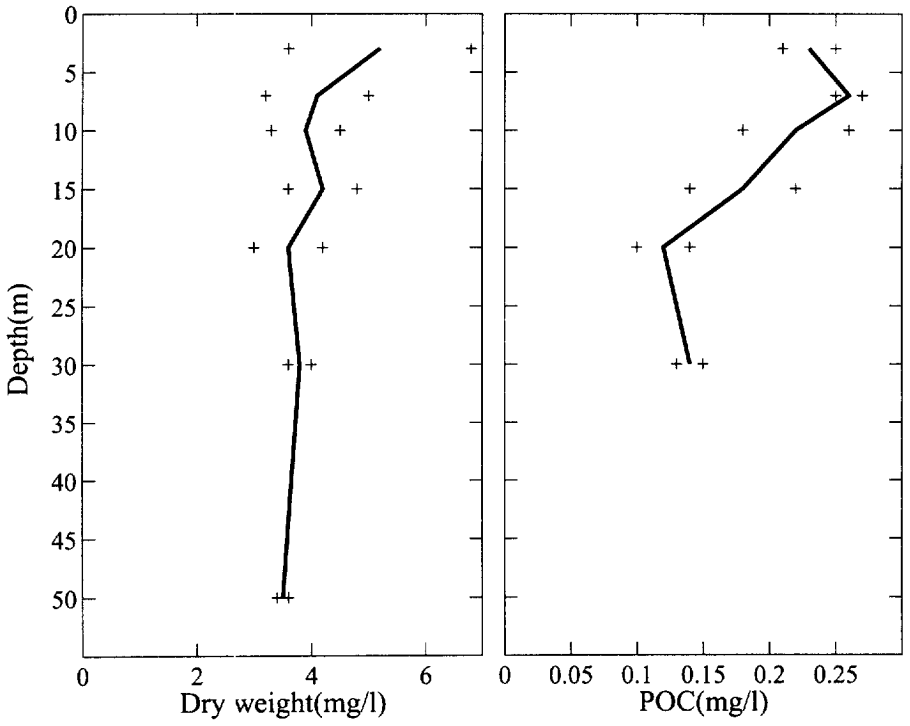

Fig. 2. Particle concentrations as captured on filters for 29 July 1993. Left: dry weight; right: POC. Chlorophyll *a* concentrations were 1.3, 1.6, 1.6, and 1.6 $\mu g\, l^{-1}$ at 3 m, 10 m, 15 m, and 30 m, respectively.

INSTRUMENTS

Aperture impedance particle counters

Coulter particle counter. The model used was a Coulter Multisizer II. Samples were analyzed using two apertures (100 μm and 400 μm) for sample volumes of 0.5 cm^3 and 100 cm^3, respectively. Results were combined by using the results for the smaller aperture for particles less than 20 μm and results from the larger aperture for larger particles. Further details have been given by Li and Logan (1995).

Elzone particle counter. The Elzone 280 particle counter is a resistance particle counter that is similar to the Coulter Multisizer II. Samples of 1 cm^3 and 3 cm^3 were analyzed using 120 μm and 380 μm aperture tubes, respectively. A further description has been given by Dam and Drapeau (1995). There was some uncertainty about whether reported data from the 380 μm aperture were particle counts for 1 or 3 cm^3. We assumed that they were for 3 cm^3 after an analysis of particle count distributions at low concentrations.

Image analysis of filtered sample

A sample volume of 15 cm^3 was filtered onto a 1.0 μm pore-size black polycarbonate

membrane filter (25 mm diameter, Poretics). Samples were stained with acridine orange before filtration; filtered samples were stained using alcian blue. Samples were analyzed using an automated image analysis system at 100 × magnification. Because only about 20% of the filter was analyzed, the effective volume sampled was actually 3 cm^3. Further details have been given by Li and Logan (1995).

In situ image analysis systems

Photographic camera. The SNOWCAM system photographed particles illuminated in a light slab formed by the collimated light from a strobed light system (Fig. 3a). The slab was 10.4 cm × 14.7 cm × 5 cm (772 cm^3). The system was tethered at the desired depth for the desired time, with natural water flow providing unsampled water for sequential photographs. Film negatives were scanned with a 1000 line video camera system and the digitized image corresponding to a volume of 0.27 l was analyzed using a computerized image analysis software system. Total sample volume at a depth ranged from 1.1 to 3.8 l. Further details have been given by MacIntyre *et al.* (1995). Values shown here represent 2 m averages (10–12, 14–16, and 30–32 m).

Confocal television systems. The Marine Aggregated Particle Profiling and Enumerating Rover (MAPPER) system uses four diode lasers (685 nm), each set at the corner of a square, and line-generator optics to create a thin (approximately 1 mm) sheet of illumination (Fig. 3b). Three longpass-filtered video cameras with different magnifications have coincident image planes in the light sheet. The MAPPER system is deployed with a loose tether, essentially falling free through the water column, sampling water that passes through the light sheet. Recorded images for each of the three cameras were processed to determine the size distribution of particles captured in the light sheet. Analysis of sequential images captured over a small depth range provided sample volumes larger than that of the light sheet.

The data from the three cameras were combined after the smallest two and largest one size categories for each subsystem were deleted, as were any values equal to zero. As data from the three systems overlap, a least-squares fit to a hyperbolic slope of a continuous distribution was calculated. This procedure discriminates against individual data points that are affected by under-sampling or a low signal-to-noise ratio. The effective volumes sampled were 3.763, 1.659, 0.184 l per meter of depth for the low, medium and high resolution cameras. The highest resolution achievable was 50 μm. Further details have been given by Costello *et al.* (1992, 1995).

The data shown in this paper have been pre-processed and, as a result, do not show the behavior at small particles sizes of the other *in situ* results. The values shown here are 2 m averages centered on the depth of comparison (9–11, 14–16, and 29–31 m).

IR laser-light sheet video system. The Particle Laser Imaging System (PALIS) is mounted on the forward underside of a remotely operated vehicle (ROV) called BORIS, for Bio-Optical Remotely operated Instrumented Submersible (Maffione *et al.*, 1993). Two IR (840 nm) laser diodes with cylindrical optics create a cross-illuminated, vertically oriented light sheet approximately 1 mm thick and 15 mm high (Fig. 3c). A high magnification video camera is focused onto the light sheet, which images the 90° light scattering by the particles passing through the light sheet as the ROV moves horizontally through the water at a fixed depth.

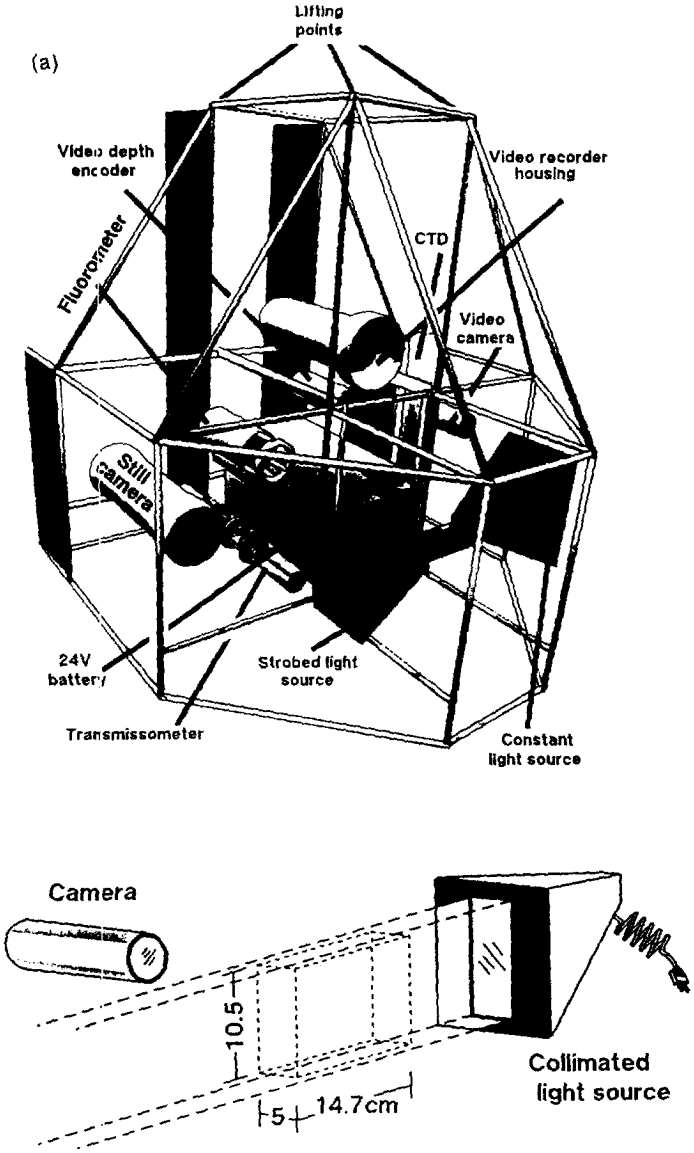

Fig. 3. Schematic diagrams of instruments. (a) SNOWCAM. Above—diagram of the entire package equipped with still and video cameras, CTD, fluorometer, and transmissometer, all powered with a 24 V battery. The vertical fins at the rear of the package orient into the local current. Below—light is passed from a strobed source through three Fresnel lenses to produce a collimated beam 5 cm thick. The camera is positioned perpendicular to the beam and images only particles illuminated within the beam. (b) MAPPER. The instrument is drawn as if the observer were looking up at the descending instrument. The four cylindrical housings (pointing inward near the bottom of the instrument) contain the diode laser projectors and optics which create the structured light sheet. Further upward on the central axis of the system is the main housing which contains the three video cameras and synchronization electronics. Other components make ancillary environmental measurements or are used for buoyancy and descent velocity control. (c) Particle Laser Imaging System (PALIS). From MacIntyre *et al.* (1995).

(b)

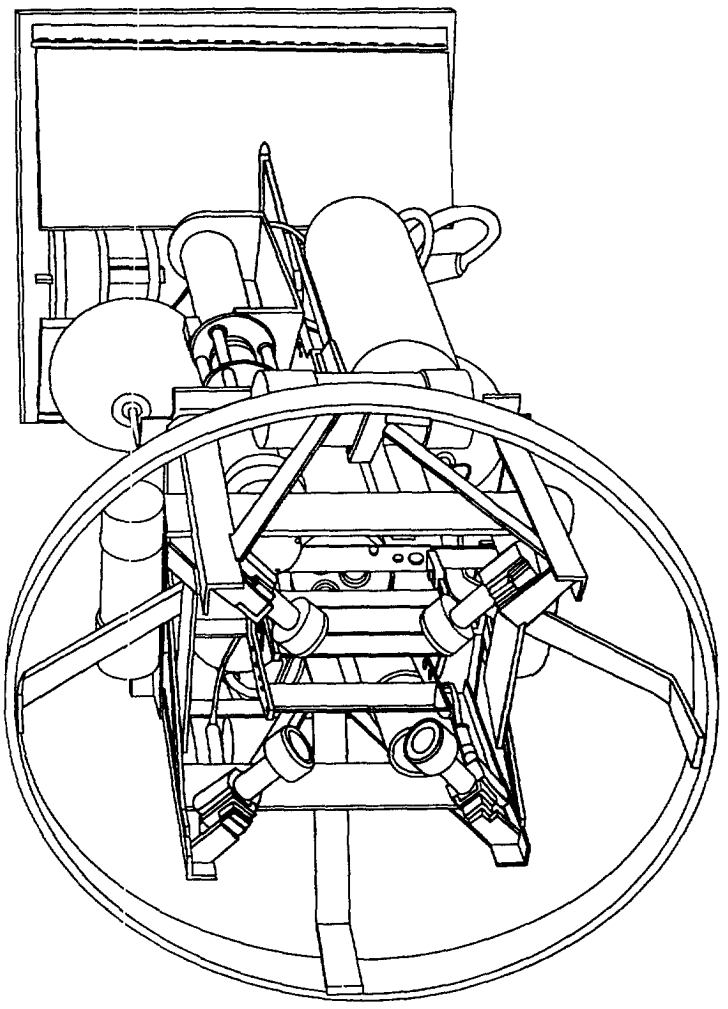

Fig. 3. *(continued overleaf)*.

The magnification setting for the data reported here resulted in a single pixel resolution of about 4 μm. The object area at the light sheet was about 1.4 mm diagonal. Particles that pass through the light sheet in the object area are sized and counted in real time with an analog video-processing circuit that adds the number of contiguous pixels above a given threshold and bins them according to their summed cross-sectional area. Because the illuminated object area is known and the speed of the ROV through the water is measured with a velocity sensor, the total sampling volume can be accurately calculated. Normalizing the particle bin counts by the size of each bin and the sampling volume, a differential particle size spectrum is produced. For the data reported here, volumes sampled ranged from 460 to 1690 cm^3. Particles smaller than 10 illuminated pixels and larger than 1 mm, or particles that

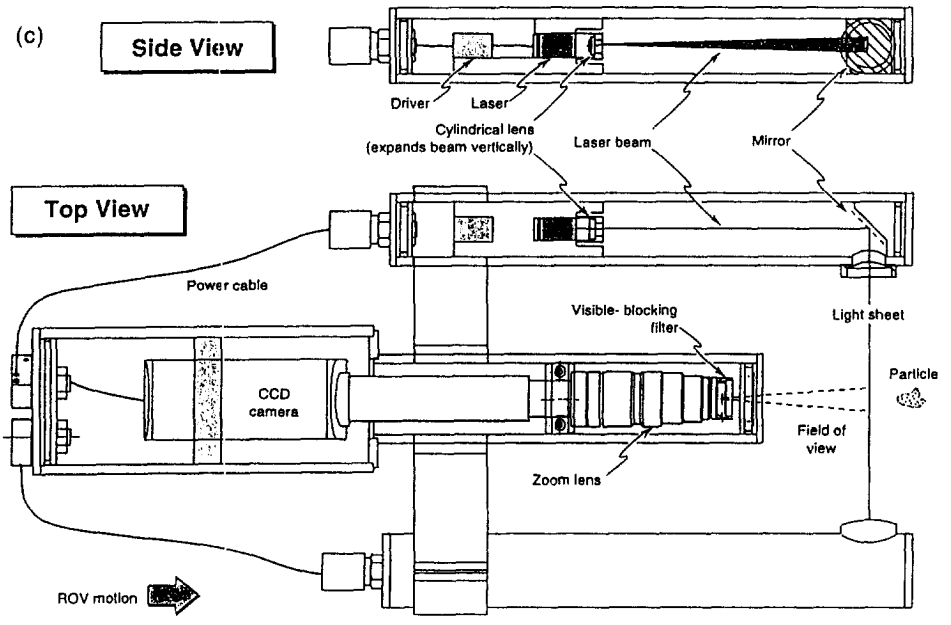

Fig. 3. (*continued*).

have more than four pixels on the edge of the image, are not counted. These criteria are somewhat arbitrary and based on empirical tests.

RESULTS

The following analysis starts with an examination of the results for individual instruments, developing a truncated data set that is used in subsequent sections. The analysis continues with comparisons of results from instruments based on the same physical principles (aperture impedance and optical imaging). It concludes with an effort to unite the two sets of data to provide common particle size spectra over almost four orders of magnitude of particle length.

Manipulation of data from individual instruments

Minimum detectable particle concentration. A constraint of any technique for estimating size spectra is that there must be at least one particle present in a size interval to be able to estimate the particle spectrum. A comparison of the results from the different instruments with such a minimum spectrum calculated as in equation (2) shows that spectra for all techniques had values at the large end of their ranges that showed the effect of too few particles (Fig. 4). The size ranges were characterized by missing values. Those values that were present were close to those for the minimum spectrum (Fig. 4). If included in the analysis, they would show a change in spectral slope for which there is no evidence. Furthermore, those spectral values calculated using few particle counts suffer from uncertainties associated with small number statistics. We have deleted all spectral values

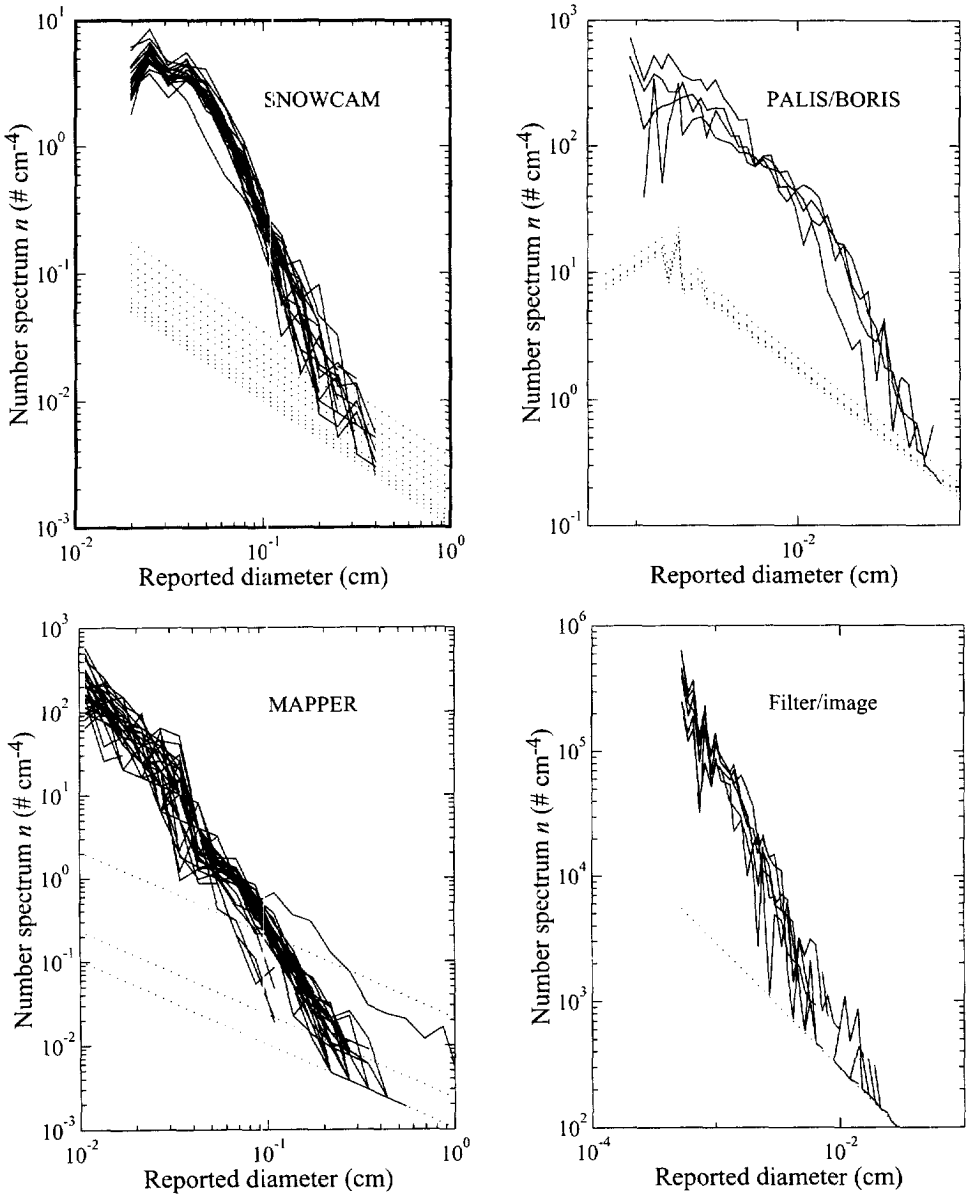

Fig. 4. Particle size spectra for the different imaging instruments as a function of size compared with the minimum detectable size spectra, n_{min}. Continuous lines represent reported spectral values; dotted lines represent n_{min}. Data represent more depths than the three emphasized in this paper. Sample volumes were not always constant between depths. Diameters are those reported for the instruments, with no attempt to convert to a common basis.

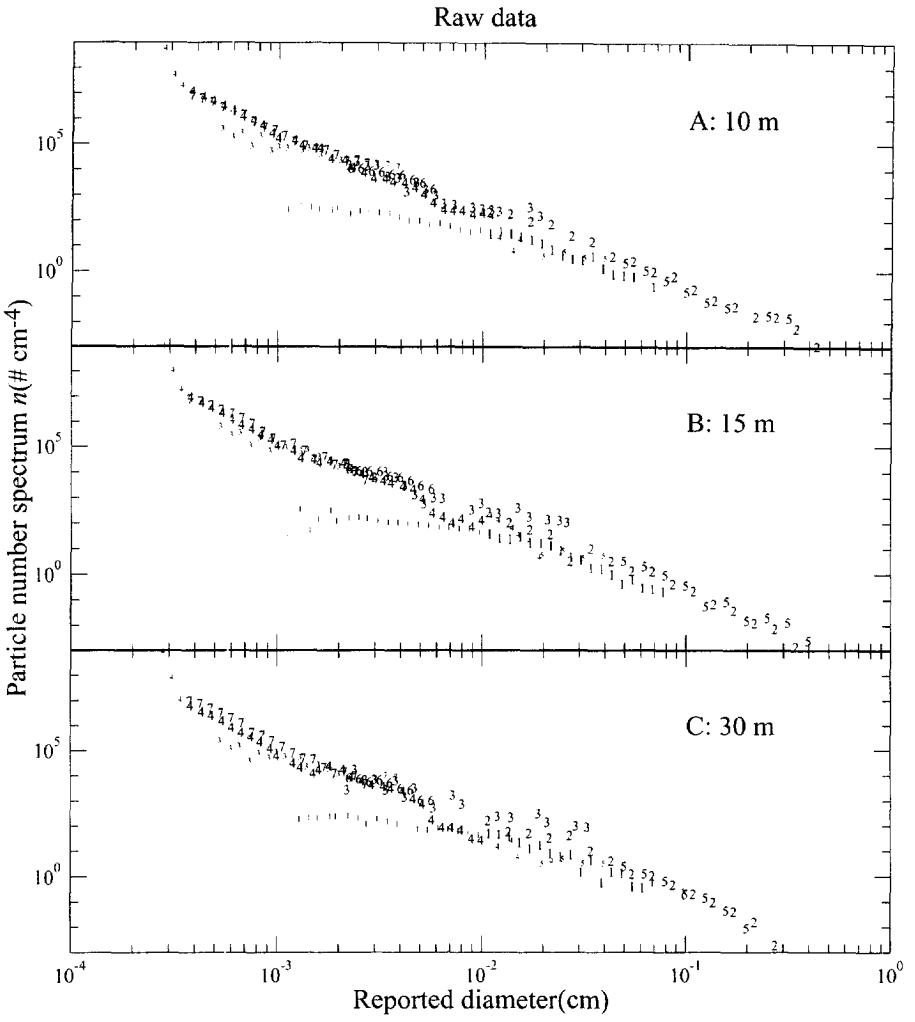

Fig. 5. Particle size spectra for all instruments after spectra were trimmed for low concentrations at large particle diameters. Small digits represent values that were dropped because they were outside the acceptable size range for the instrument. Data were for PALIS (1), MAPPER (2), filter/image (3), Coulter Counter (4), SNOWCAM (5), Elzone 380 μm orifice (6), Elzone 120 μm orifice (7). Diameter as in Fig. 4.

that occurred at particle diameters larger than the smallest size interval with a zero value for that spectrum.

Minimum detectable particle size. All particle sizing techniques suffer from weak signals from small particles. For an aperture impedance counter this can manifest itself as very large increase in counts as instrumental noise overwhelms particle signal; for image analysis systems it shows as a loss of particle counts (Fig. 5). In either case, there is a change in

spectral slope at the lower limit of particle size. A comparison of raw results from different instruments that are not at the end of their ranges shows that these slope changes are not real (Fig. 5). We have removed the offending spectral values for the small sizes from the spectral records by setting a lower diameter limit of 3.8 μm for the Coulter Counter, 100 μm for PALIS, and 400 μm for SNOWCAM data.

The expected relationship resulting from fractal scaling and the slopes of the particle spectra imply that the spectral values obtained by image analysis of filtered samples should not be much smaller than that of the Coulter Counter (see Appendix A). Because particles smaller than about 20 μm had lower spectral values for the image data than for Coulter Counter, their spectral values for smaller diameters may have been biased. To avoid potential problems, spectral values from the image analysis systems were dropped for particle diameters less than 20 μm. The resulting set of sanitized data was used for all further calculations.

Comparison of in situ instruments

Results from *in situ* imaging instruments show differences that are large (a factor of ten) if spectral values are compared at a given diameter but smaller if the particle diameters are compared at a given spectral value (Fig. 5). We expect that most large particles will be observed by each of the different instruments. However, the diameter that is assigned to a given particle by an imaging system is a function of the system sensitivity, threshold settings, particle reflectivity, shape, and other factors (e.g. Costello *et al.*, 1994, 1995). The problem arises because the rapid decrease in particle concentration with increasing particle size results in large errors in spectral values for small biases in the estimation of particle diameter. For example, if $n \propto d^{-3}$ and the estimated diameter is 1.5 times the real one, the estimated n will be $1.5^3 = 3.4$ times the real one.

The effect of different instruments assigning slightly different diameters to the same particles can be investigated with a simple analysis. If the diameter reported for one system d_2 is a constant multiple of that of another d_1 then $d_2 = \alpha d_1$, where α is the multiplicative factor relating the two. If the spectra are given by equation (4) ($n_1 = a_1 d_1^{-b}$; $n_2 = a_2 d_2^{-b}$) and the two spectra are related by equation (1) (i.e. $n_1 = \alpha n_2$), then algebraic manipulations yield

$$\log \alpha = (b - 1)^{-1}(\log a_2 - \log a_1). \tag{9}$$

When we transformed the different spectra, there was enough variability in the fitting process that different image systems yielded different values of b (Table 2), even though the graphs show no distinct differences in slopes (Fig. 5).

We therefore modified our approach, assuming that the slope of the longest record (that of the MAPPER) was representative of the other two instruments at a given depth. Then, for each instrument a was calculated as

$$\log a = \text{average}(\log n + b \cdot \log d) \tag{10}$$

where b came from the longest record and the values of n and d were for that instrument. The results are that the diameters for particles measured by BORIS and SNOWCAM are 56% and 103% of the diameters for the same particles reported by MAPPER. Thus, the spectra from the different instruments differ in ways that can be understood as resulting from relatively small differences in the diameters that they assign to the same particles.

Table 2. Results from linear regressions

Parameter	10 m	15 m	30 m
MAPPER			
log a	−3.85	−3.99	−3.97
b	3.31	3.26	3.27
α	–	–	–
BORIS			
log a	−3.69	−3.27	−2.81
b	2.74	3.27	2.81
α	0.47	0.60	0.60
SNOWCAM			
log a	−4.44	−3.87	−4.54
b	3.69	3.37	3.87
α	0.82	1.25	1.03
Elzone—120 μm			
log a	−4.52	−6.04	−6.71
b	3.34	3.81	4.01
Elzone—380 μm			
log a	−0.90	−0.88	−2.23
b	1.90	1.92	2.36
Coulter combined			
log a	−5.03	−5.17	−5.58
b	3.50	3.49	3.57
Filter/image			
log a	−4.65	−4.06	+0.22
b	3.41	3.14	1.38
Combined/optical diameter			
log a	−3.45	−3.69	−3.61
b	2.96	3.00	2.97

Coefficients for linear regressions on log-transformed particle size spectra: $\log n = \log a - b \log d$, where $\log x \equiv \log_{10} x$ and a has units of cm. α is the ratio of given diameter to MAPPER diameter. It was calculated after estimating a as the mean value of $(\log n - b_M \log d)$, where b_M is the value of b at the same depth as determined for the MAPPER data. The combined/optical data include both data from optical instrument (MAPPER) as well as data from the Coulter Counter transformed to an optical diameter basis using equation (11) (Fig. 12).

Comparison of aperture impedance instruments

The spectra determined using the two apertures on the Elzone do not always superimpose, although the differences in spectra were within a factor of two (Fig. 6). Similar differences have arisen when combining the 100 μm and 400 μm aperture spectra in the Coulter Counter (X. Li, personal communication, 1996). Hunt (1980b) has observed a similar problem.

Elzone spectra made using the 120 μm aperture for particle diameters 21 μm or less were combined with those from the 380 μm aperture for particle diameters between 22 and 50 μm. The resulting spectra are very similar to those obtained using the Coulter Counter, although there are differences (Fig. 6). First, the spectra increasingly diverge with depth, going from almost indistinguishable differences for samples from 10 m depth to being a factor of three different at 30 m. This changing difference could result from instrumental drift during the course of the measurements, with the diameters from the Coulter and Elzone changing by

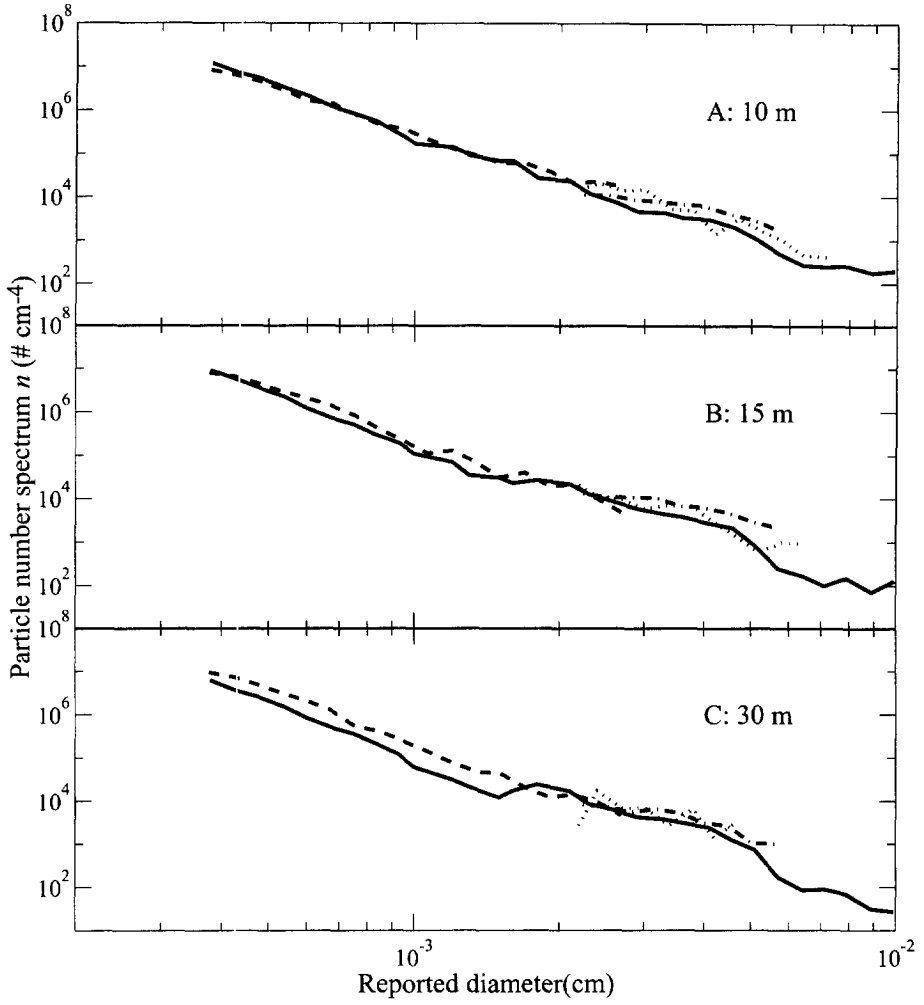

Fig. 6. Particle size spectra for the laboratory particle sizing instruments. Symbols: Coulter Counter (continuous line); Elzone particle counter with 120 μm orifice (dashed line); Elzone particle counter with 380 μm orifice (dot–dashed line); filter/image analysis system (dotted line).

only 10%. Second, local maxima in size space for the spectra from the Coulter Counter are not evident in the spectra from the Elzone.

Comparison of aperture impedance and image analysis instruments.

Before the spectra calculated using data from the imaging instruments can be compared with those calculated using data from the aperture impedance instruments, the particle diameters and spectra must be equivalent. Because the imaging instruments measure a diameter akin to the diameter of gyration and the aperture impedance instruments a diameter akin to that calculated from the conserved volume (or mass), their measures of

particle size differ. The fundamental assumption of this analysis is that the diameter assigned to a particle measured using an aperture impedance instrument is the conserved volume equivalent, d_c, whereas that assigned using an optical system is an apparent diameter $d_I = (0.6)^{-0.5} d_g$. The constant $(0.6)^{-0.5}$ sets the values of the two diameters to be the same for the single spherical source particle (equation (8)).

Equation (5) can be manipulated to yield

$$d_c = B d_0^{1-D/3} d_g^{D/3} \tag{11}$$

where d_0 is the diameter of the hypothetical monomer and B is a constant. For a solid sphere, d_g is $0.6^{0.5}$ times its diameter. We have set $B = 0.6^{-D/6}$ for equation (11) to be valid for the solid single particle. Given values of d_0 and D, spectra from an aperture impedance particle counter and an imaging system can be related. Unfortunately, the reported values for d_0 and D vary greatly and cannot be used in the present situation (e.g. Li and Logan, 1995; Jackson *et al.*, 1995).

We have estimated the values of d_0 and D that apply here by finding those values that make the best fit between particle size spectra from the aperture impedance instrument and transformed spectra from the imaging systems.

Minimizing the differences in overlap regions. To find these optimal values, we first calculated what the diameters and spectral values n_I would be in conserved volume equivalents if reported diameters were the diameters of gyration for the given values of d_0 and D by using equation (11) and a suitable version of equation (3) on the diameters d_I and particle size spectral values n_I. The resulting diameters and particle size spectra were log-transformed. The region of log-diameter overlap was divided into ten equally spaced intervals and the values of log n calculated by linear interpolation for each spectrum at the 11 division points. The r.m.s. difference between the spectra σ was calculated as

$$\sigma = \left[\frac{1}{11} \sum_{j=1}^{11} (\log n_{I,j} - \log n_{C,j})^2 \right]^{0.5} \tag{12}$$

where $n_{C,j}$ represents the spectral estimate from the aperture impedance instrument (usually the Coulter Counter) and $n_{I,j}$ the transformed image value at the jth particle diameter. The goal was to find the values of d_0 and D that minimized the difference function σ.

The transformation of n_I caused the minimum particle diameter for the image data to decrease but did not always allow the overlap of a large enough region to make a reasonable comparison. As a result, only transformations with an overlap that included at least four data points from the aperture impedance region were used. Because the data set that used the Elzone counts did not extend beyond 50 μm particle diameter, it did not provide enough overlap with the transformed image data to be useful. As a result, only the Coulter Counter data were used for the aperture impedance region in these comparisons. Similarly, the MAPPER system provided the only *in situ* data set that extended to small enough sizes to be useful over a sufficient range of d_0 and D. The MAPPER data were combined with the image data from the filtered samples to obtain an adequate size range, although the MAPPER data were also used alone.

The graph of σ as a function of D and d_0 for the combined imaging data shows a region bounded by $1 \leq D \leq 3$ and 1 μm $\leq d_0 \leq$ 20 μm for the 10 m sample (Fig. 7). The best fit, that

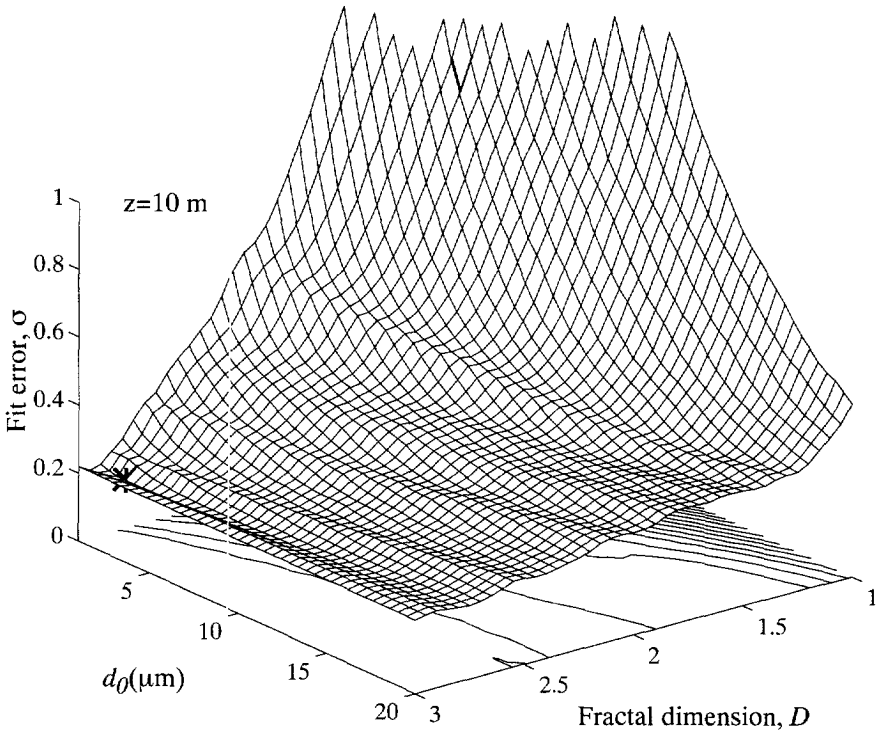

Fig. 7. Fit error σ in the region of overlap for Coulter Counter and combined MAPPER plus filtered particle data at 10 m for different transformations of the image data. The lower figure is a contour of the overlying three-dimensional figure. The minimum value, at $D = 2.65$ and $d_0 = 1.5$ μm, is indicated with an asterisk.

with the minimum σ, was for $d_0 = 2.4$ μm and $D = 2.9$ (Fig. 8a). The relationships at 15 m were similar, although the best fit was for $D = 2.3$ and $d_0 = 1$ μm. The relationship at 30 m was more complicated. There were several regions with local minima for σ, one similar to those at 10 and 15 m depth (not shown), as well as one with lowest minimum, for $D = 2.1$ and $d_0 = 13.3$ μm (Fig. 8c).

The best fits for imaging particle spectra were less reliable without the filter data because of the limited region of overlap. However, the best fit values of σ were for $D = 2.5$, 2.55, and 1.45 and $d_0 = 2$, 1, and 19.5 μm for the same parameter ranges at 10 m, 15 m, and 30 m depth, respectively. These values are less reliable because of the more limited overlap range, but are similar to those calculated using the combined image data.

Constraining the minimization with particle concentration. One problem with this approach is that there was not a d_0, D pair that was clearly the best because the surface formed by plotting σ as a function of d_0 and D has a large, fairly flat region rather than one value of σ that is clearly the smallest and the "best" (Fig. 7). The conservative volume of a particle estimated from d_1 changes with the values of d_0 and D. Decreasing the value of D for a given d_0 decreases the particulate mass volume because it increases the particle porosity of a given size particle. To restrict the choices, we used the additional information available

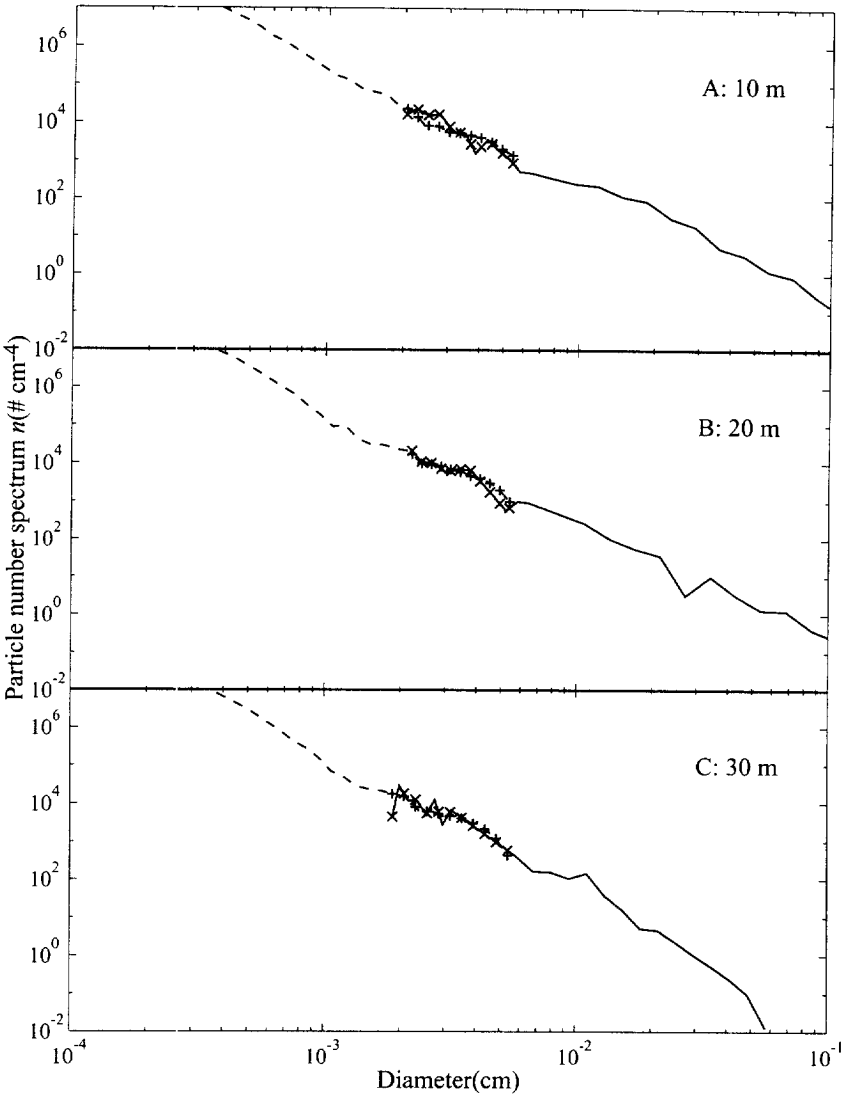

Fig. 8. Combined spectra in terms of conserved diameter for the best fit transformations of imaging data. Symbols: filter/image analysis system (continuous line); Coulter Counter (dashed line); interpolated points from transformed image (×) and Coulter Counter (+) used to calculate σ.

from the total POC measurements to provide an additional constraint on the values of d_0 and D, thereby improving the estimates of their values. We converted total POC values for a given particle size spectrum to total conserved particulate volume by using the algal carbon to volume ratios for diatoms ρ_C measured by Strathmann (1977):

$$\rho_C = \frac{C(\text{pg})}{V(\mu\text{m}^3)} = 0.44 d(\mu\text{m})^{-0.726} \tag{13}$$

where V is the volume of an algal cell and C is its carbon content. Because this ratio depends on d, we have assumed that $d = d_0$, the diameter of the unit particle, when converting POC concentrations to total particulate volume. Total conservative volume for a given POC concentration is

$$V_{TC} = P_C/\rho_C \tag{14}$$

where P_C is the POC concentration. The total conservative volume V_{TS} can be calculated from the spectrum n_c by numerically integrating:

$$V_{TS} = \int \frac{\pi}{6} d_c^3 n_c \, dd_c. \tag{15}$$

The values n_c can be calculated from n_I for given values of d_0 and D using equation (1) and equation (3).

The values of D and d_0 for which the integrated volume equals the suspended solids volume describe a constant-volume curve on the σ surface (Fig. 9). The values of D and d_0 that minimize the value of σ along this curve provide the best estimates consistent with the suspended particle concentrations (Fig. 10). The minimum values of σ subject to this constraint occur when $d_0 = 9.55$, 6.70, and 3.38 μm and $D = 2.28$, 2.36, and 2.26 at 10 m, 15 m, and 30 m, respectively (Fig. 11). Results are more consistent between depths than are those for the approach taken earlier.

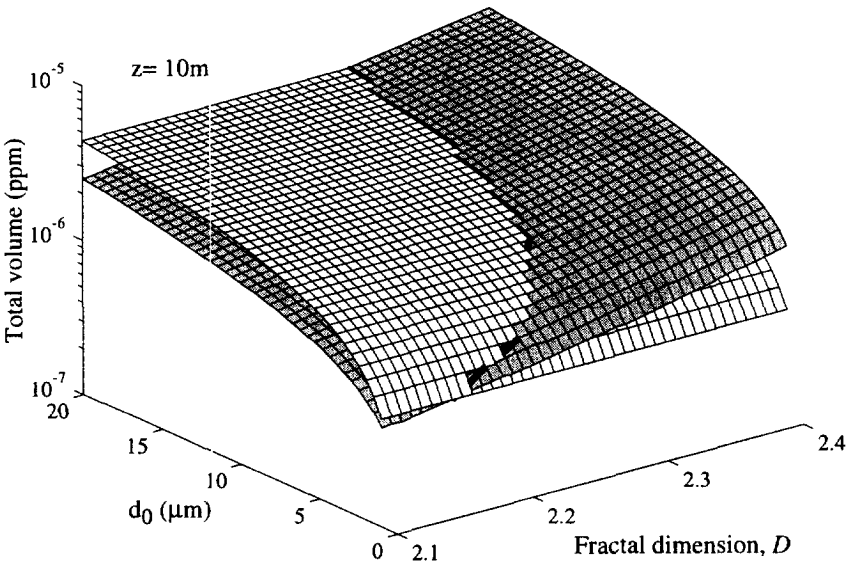

Fig. 9. Integrated volume as a function of fractal dimension and monomer size for 10 m samples. The horizontal plane represents V_{TC}, the particle volume/sample volume calculated from POC measurements for a given value of d_0. The tilted surface represents V_{TS}, the integrated volume calculated after the image data were transformed using the values of d_0 and D to the conserved volume assumed to be measured by the Coulter Counter. The intersection of the two surfaces provided the values of D and d_0 that were applied to the preceding figure to yield the constant volume curve.

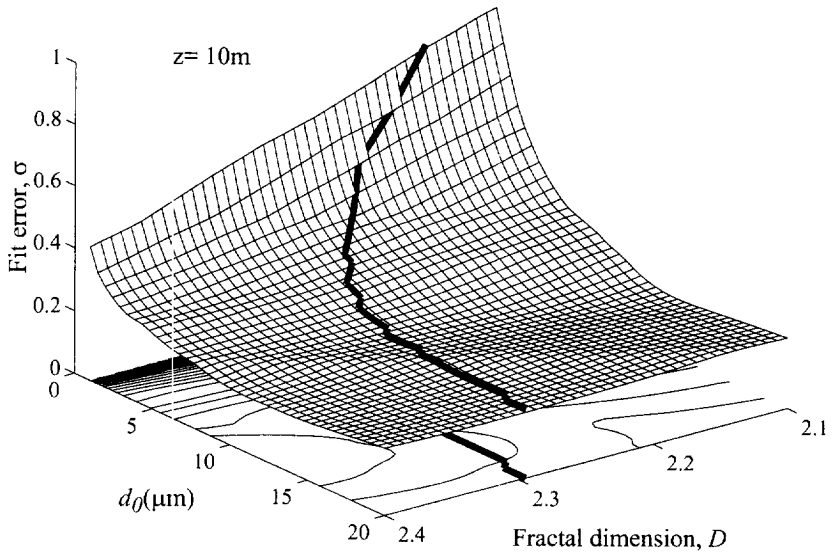

Fig. 10. Fit error σ in the region of overlap for Coulter Counter and transformed MAPPER plus filtered particle data at 10 m showing the curve of constant volume. The minimum value is at $D = 2.28$ and $d_0 = 9.55$ μm.

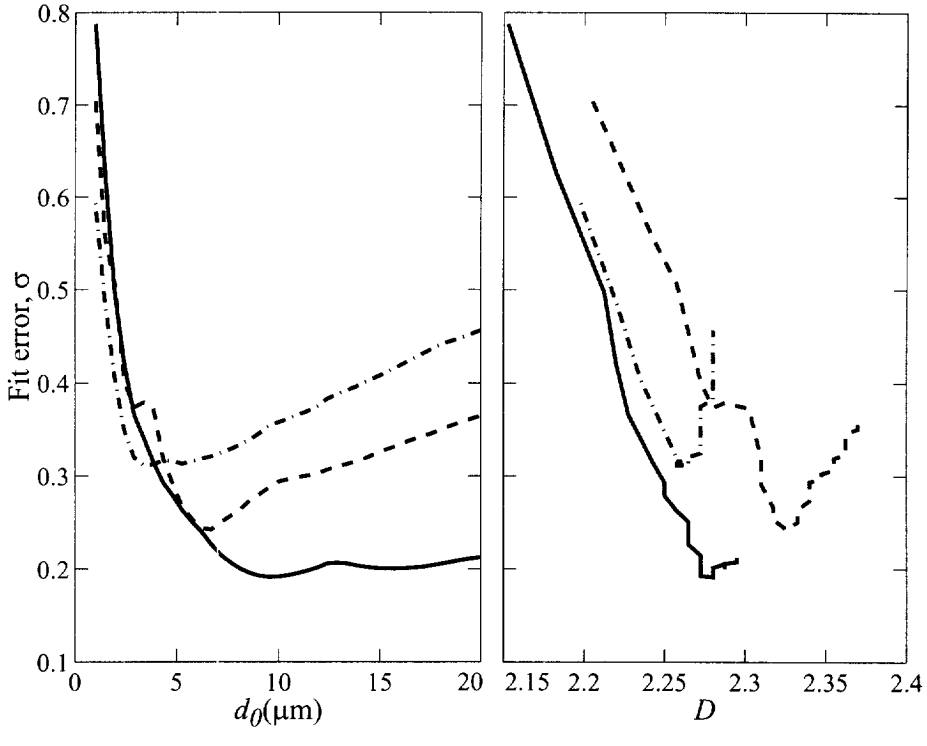

Fig. 11. Values of σ along the constant volume curve as functions of D (left) and d_0 (right) for 10 m (continuous line), 15 m (dashed line), and 30 m (dot–dashed line).

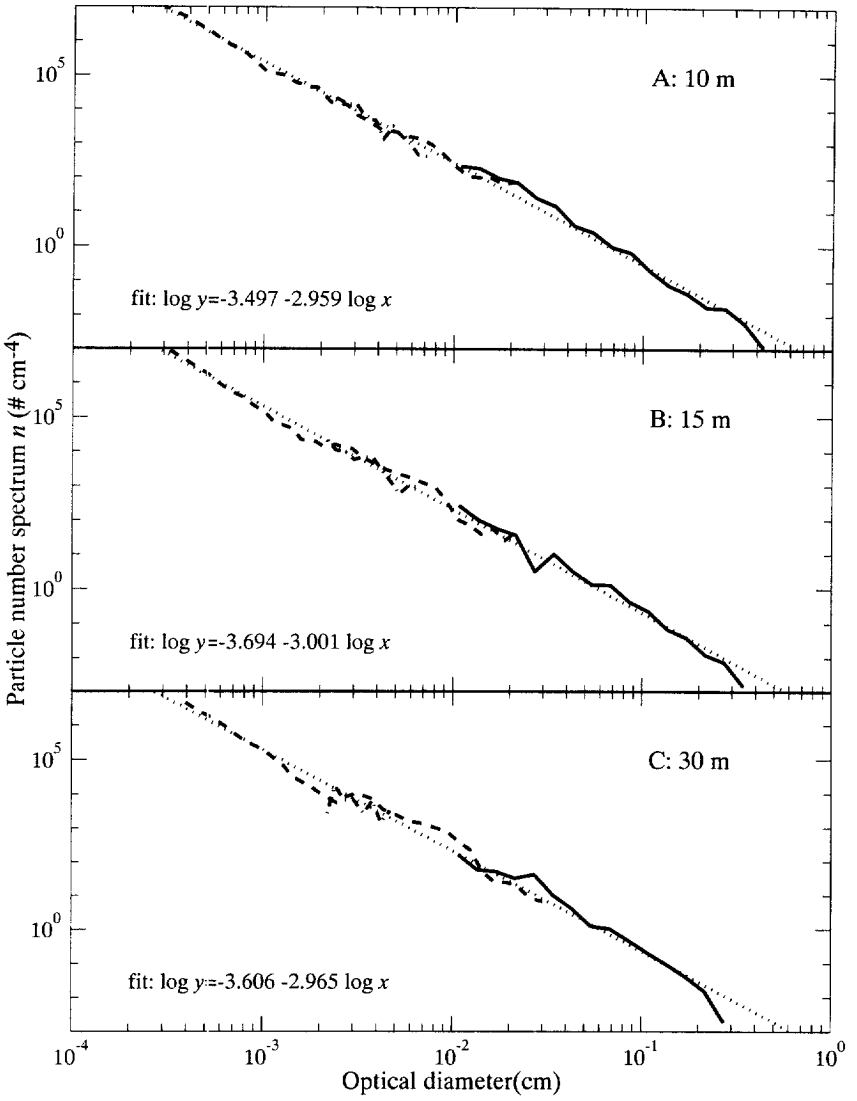

Fig. 12. Particle size spectra converted to common basis of optical particle diameter (n_1 as a function of d_1) using the values discussed in the text. D and d_0 as in previous figure. The dotted lines represent the best fit line of the form $\log n = -b \log d + \log a$, with $b = 2.959$, 3.001, and 2.965 for depths of 10 m, 15 m, and 30 m, respectively. MAPPER data (continuous line); Coulter Counter data (dashed line); image analysis data of filtered samples (dot–dashed line).

Best estimate combined spectra. The combined number spectrum over a size range of 10^{-4} to almost 1 cm shows the customary decrease of particle number (Fig. 12). The data provide a nearly straight line in the logarithmically transformed data. Linear fits to the logarithmically transformed spectra and diameters yield slope values of 2.959, 3.001, and 2.965 at 10 m, 15 m, and 30 m, respectively.

Such near-linearity in the particle number spectrum is deceiving because the large spectral

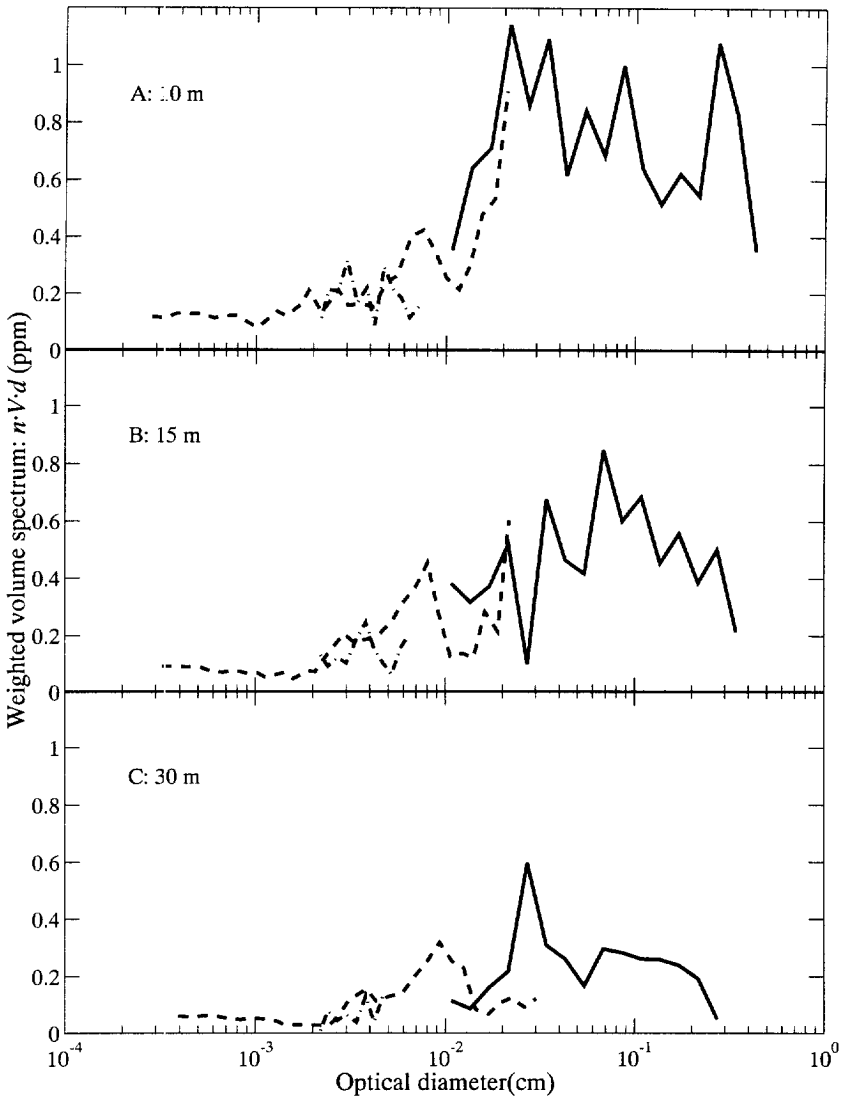

Fig. 13. Distribution of mass (conserved volume) as a function of apparent (optical) size. The volume is that that a particle has after the fractal transformation (equation (11)). The y-axis is a normalized volume distribution, calculated by multiplying the volume distribution $v_C n_I$ by the image diameter d_I. The transformation forces the area under a curve in this figure (with the log d_I x-axis) to be proportional to the conserved volume for particle in that range. $d_I/d_g = 1.29$. Top: 10 m, $D = 2.28$, $d_0 = 9.55$ μm; middle: 15 m, $D = 2.33$, $d_0 = 6.70$ μm; bottom: 30 m, $D = 2.26$, $d_0 = 3.38$ μm. MAPPER data (continuous line); Coulter Counter data (dashed line); image analysis data of filtered samples (dot–dashed line).

range of about 12 orders of magnitude masks changes that are small relative to this range but that are important in determining mass distribution. A calculation of the mass distribution across the size range shows that most of the mass is in the larger size range, greater than 100 μm (Fig. 13). Furthermore, there is a decrease in particle mass at sizes

greater than 2–3 mm that suggests most of the particle mass is contained in the sampled range.

The value of b in the relationship $n = ad^{-b}$ is different if the conserved volume equivalent diameter d_c is used rather than d_I. From the fact that $d_I = c_1 d_c^{3/D}$ and equation (1), it follows that

$$n_c = n_I \cdot \frac{dd_I}{dd_c} = c_2 d_I^{-b_I} \cdot c_3 d_c^{(3/D)-1} = c_4 d_c^{-[(3b_I/D)-(3/D)+1]}$$

where c_1, c_2, c_3, and c_4 are constants. It follows that n_c can also be expressed as in equation (4) with

$$b_C = \frac{3b_I}{D} - \frac{3}{D} + 1 \tag{16}$$

where the subscripts C and I refer to the conservative (Coulter Counter) and image diameters. Applying this relationship results in estimates for $b_c = 3.58$, 3.58, and 3.61 at 10 m, 15 m and 30 m, respectively. Thus, the slope when using the conserved volume equivalent typical of Coulter Counters is greater than those shown in Fig. 12 by about 0.6.

DISCUSSION

The availability of six different particle measuring instruments in a region with large aggregates has allowed us both to examine the results of such measurements and to combine them, constructing a particle size spectrum that spans nearly four orders of magnitude. As part of the process, we have learned about the measurement of particle size spectra.

Measurement of particle size

Particle characterization and subsequent calculation of particle size spectra uses an amalgamation of a binary measurement (presence or absence of a particle) coupled with a quantitative estimate of particle size. The nature of these two types of measurements has important implications for the calculation of particle size spectra.

First, the minimum estimate of particle concentration is that for which there is only one particle present in a sample volume. The experimental results show that the most important constraint on the maximum particle size for which we can estimate the particle size spectrum is sample volume. As a result, the probability of capturing a suitable particle within a given volume at a particular concentration can be more important for the spectral measurement than the maximum size particle an instrument can handle. All the instruments whose results we analyzed showed the characteristic signs of too small a sample volume to fully use their particle sizing capabilities.

Second, relatively small differences in estimating particle diameters can result in large differences in estimating particle spectra because the particle size spectrum decreases so rapidly with increasing particle size. This characteristic of particle size spectra leads inescapably to potentially large errors in measurements of absolute particle size distributions, although this need not affect the estimates of the slope (b).

Aggregates accentuate the problem of diameter measurement because particle diameter can be characterized by several methods—including the spherical-equivalent diameter for

the conserved volume, the diameter of gyration, and the encased diameter—that differ slightly. We have assumed that the diameter that is reported by an image analysis system is proportional to the diameter of gyration, but have not proven it. This assumption is, however, consistent with past experience with imaging systems (e.g. Rogak and Flagan, 1990; Logan and Kilps, 1995).

In all of this analysis, there is the implicit assumption that the results reported for any instrument are representative of the actual particle spectrum, even if the interpretation of the reported particle size is unclear. McCave (1984) has shown that the shear associated with flow through the aperture of a Coulter Counter can cause larger aggregates to break up and add a spurious peak to the particle size distribution. In his case, the peak was formed at a reported diameter of 16 μm. Jiang and Logan (1996) have noted the actual diameter of an aggregate is frequently larger than that reported by a Coulter Counter because of the fractal scaling and could be larger than the aperture diameter despite being within the usually accepted size range of validity. As a result, these larger particles are especially susceptible to aperture shear disaggregation. Jiang and Logan recommended that only information for particles with diameters less than 20% of the aperture diameter be used to avoid the problem. This recommendation is consistent with McCave's observation of disaggregation artifacts in the particle size spectrum at a size 23% of the aperture diameter of 70 μm.

We did, in fact, omit particles in size ranges where the size spectra showed evidence of having substantial artifacts. We used only data from the Coulter Counter aperture for particles that were less than 20% of the 100 μm and 25% of the 400 μm aperture sizes. This data winnowing, along with the consistency between the results collected using the 100 and 400 μm apertures, suggests that our results were not influenced by aperture shear.

Particle porosity and the fractal description

We have assumed that the aperture impedance instruments measure conserved mass, the solid part of a permeable particle. There is evidence that the sizes reported by such instruments do depend partly on the particle geometry, both for solid particles of different shapes (e.g. Lloyd, 1982; Lines, 1992) and for porous particles (Eckhoff, 1969; Treweek and Morgan, 1977; Van der Plaats and Herps, 1984). These published reports suggest that volume reported for a particle should be within a factor of two of that for a solid sphere with the same conserved volume. This translates to an uncertainty in d_c of $2^{1/3} = 1.26$.

The calculations of fractal scaling made here implicitly assumed that aggregates were composed of monomers the same size as algal cells. Such an assumption worked well in the analysis of aggregates in a mesocosm of aggregating diatoms and appears to be reasonable for aggregates in the diatom-dominated region of Monterey Bay.

The fractal dimensions calculated here, 2.2–2.3, are similar to the 2.3 estimated for larger particles in a mesocosm experiment (Jackson *et al.*, 1995), but larger than the 1.7–2.5 estimated using the Coulter Counter and the optical/filter data (Li and Logan, 1995; Li *et al.*, 1997). Such differences could result from biases in the different techniques but may also result from different processes being important in different parts of the size spectrum. Such an idea has been suggested by Risović and Martinis (1996), who have estimated fractal dimensions of suspended particles in seawater by a light scattering technique. They argued that the value of D is 1.7 ± 0.1 for particles smaller than 2.5 μm and 2.7 ± 0.4 for larger particles. Although fractal scaling with a monomeric particle having $d_0 = 10$ μm may work well to explain the distribution of aggregates as large as 1 mm, it does not explain the

existence of particles smaller than 10 μm. Aggregates of such small size must be formed by the collision of smaller particles. The size dependence of collision mechanisms and the different fractal dimensions associated with them must be considered.

The use of particulate carbon concentrations when estimating the fractal parameters for the particles resulted in estimates for D and d_0 that were surprisingly uniform through the depth ranges. Such uniformity is a reassuring aspect of these results.

Even if the aggregates are formed from one source particle here, there is no reason for this to be true in other areas. Microscopic images of particles sampled in the benthic boundary layer show a heterodisperse mixture of particles (McCave, 1984). Furthermore, the images show that the relative composition varies with particle size, with smaller aggregates having relatively more mineral particles and the larger particles having more organic matter. This analysis may work for the surface waters of Monterey Bay because of the dominance of algal particles.

Particle size spectra over the large range

Particle size spectra have usually been measured with just one instrument, typically an aperture impedance counter, over a particle size range of 1–100 μm (e.g. McCave, 1983, 1984, 1985; Eisma, 1986; Sternberg *et al.*, 1988). Over such ranges, the spectra often are well fitted by power series relationships. For example, McCave (1983) observed that the slope for samples taken in the benthic nepheloid layer had values equivalent to b_c ranging from 3.61 to 4.22 and having a mean of 4.0 over the particle size range 1.5 μm $< d_c <$ 12 μm. The simple fit was interrupted by a change in slope later attributed to an artifact of aperture shear disaggregation (McCave, 1984).

It is intriguing that measurements over the larger range presented here are reasonably described by a simple power law function over the entire range and that the estimates of b for the three depths are virtually the same. Furthermore, the values of b_c are similar, if in the lower range, to McCave (1983) values observed for the particles in the 1–10 μm range.

This relatively simple fit to the number spectrum is deceptive because small deviations from the power law fit are very significant. The most striking one is that most of the particle mass is in particles larger than 100 μm. Furthermore, there was significantly more integrated mass at 10 m than at 30 m (Fig. 13).

The decrease in particle mass for particles larger than about 2 mm is consistent with observations by divers. This upper size limit and the accumulation of particle mass in the larger sizes is similar to the situation observed in a mesocosm experiment (Jackson *et al.*, 1995). The accumulation in the mesocosm was attributed to a balance between aggregation processes that form larger particles and disaggregation processes that break down larger particles preferentially (Jackson, 1995). The similarity in particle mass distributions suggests that disaggregation was an important process in determining particle mass distribution at Monterey Bay as well. Such disaggregation places an effective limit on particle sizes.

Disaggregation of marine aggregates is a function of particle size and shear rate (Alldredge *et al.*, 1990). It is also a function of the strength of the ties between particles composing an aggregate, which can be altered by bacterial decomposition (e.g. Smith *et al.*, 1992).

Sheldon *et al.* (1972) and Sheldon and Kerr (1972) argued that there were equal volumes of particles in equal logarithmic size intervals up to meters. Their arguments were based on data collected using Coulter Counters for the 1–100 μm size range and general organism

abundance data for larger particles. Rodriquez and Mullin (1986) found similar biomass concentrations of zooplankton in logarithmic size intervals (upper lengths twice those of lower lengths). Although there may be such an even distribution of organisms up to meter sized animals, it appears to be unrelated to the algal and detrital particles affected by coagulation processes. The maximum observed in particle volume distribution (Fig. 13) implies that particles are not abundant at arbitrarily large particle sizes.

Environmental implications

Because particle size is so important to the functioning of marine ecosystems, the finding that most of the particulate mass is in relatively large aggregates affects our understanding of the Monterey Bay system. Trent *et al.* (1978) measured chlorophyll and phaeophytin in diver-collected aggregates and in the water column, concluding that a substantial amount of material could be in the aggregates greater than the minimum observable by divers, about 1 mm in diameter. We find that most of the particulate material is larger than 100 μm, with most of this in the 100 μm–1 mm size class that divers could not sample.

The fact that most of the particulate matter is in the larger aggregates rather than isolated algal cells implies that it should sink at speeds on the order of 100 m day^{-1} (Alldredge and Gotschalk, 1989) rather than the 2 m day^{-1} that would be more characteristic of solitary algae (e.g. Smayda, 1970). This should result in a 50 times faster settling loss rate.

The presence of so much matter in large aggregates affects the size-hierarchy of marine food webs. Larger crustaceans do feed on aggregates (e.g. Lampitt *et al.*, 1993). The abundant *Euphausia pacifica* can be expected to feed on diatom aggregates in Monterey Bay (e.g. Dilling *et al.*, 1998). Smaller organisms form their own communities within the aggregates (e.g. Caron *et al.*, 1986; Smith *et al.*, 1992; Shanks and Waters, 1996). The presence of most mass in the larger aggregates suggests that those organisms specializing in living in and on aggregates can form an important part of the planktonic ecosystem.

CONCLUSIONS

The availability of simultaneous measurements of particle size distributions has allowed us both to compare the different results and to combine them into information on the particle size spectra that spans a length range of almost four orders of magnitude. The results show that most of the particulate mass in our samples was in the larger size fraction. Such distribution is in accord with a system in which aggregation of small particles into large ones and disaggregation of the largest particles into somewhat smaller particles dominate.

Acknowledgements—We would like to acknowledge the assistance of D. Drapeau, C. Gotschalk, and X. Li in the data collection. We would like to thank Paul Hill and an anonymous reviewer for helpful critiques. This work was supported by the Office of Naval Research (N00014 87-K0005, N00014-88-J-1017, N00014-89-J3206, N00014-91-J-1249, and N00014-93-1-0226). The results were part of the SIGMA program.

REFERENCES

Alldredge, A. L. and Gotschalk, C. C. (1989) Direct observations of the mass flocculation of diatom blooms: characteristics, settling velocities and formation of diatom aggregates. *Deep-Sea Research*, **36**, 159–171.

Alldredge, A. L., Granata, T. C., Gotschalk, C. C. and Dickey, T. D. (1990) The physical strength of marine show and its implications for particle disaggregation in the ocean. *Limnology and Oceanography*, **35**, 1415–1428.

Alldredge, A. L., Gotschalk, C., Passow, U. and Riebesell, U. (1995) Mass aggregation of diatom blooms: insights from a mesocosm study. *Deep-Sea Research II*, **42**, 29–45.

Avnir, D. (1989) *The Fractal Approach to Heterogeneous Chemistry*. Wiley, New York, 441 pp.

Caron, D. A., Davis, P. G., Madin, L. P. and Sieburth, J. McN. (1986) Enrichment of microbial populations in macroaggregates (marine snow) from surface waters of the North Atlantic. *Journal of Marine Research*, **44**, 543–565.

Costello, D. K., Carder, K. L. and Hou, W. (1992) Structured visible diode laser illumination for quantitative underwater imaging. In *Ocean Optics XI, Proceedings of the SPIE, 1750*, ed. G. D. Gilbert, pp. 95–103. Society of Photo-optical Instrumentation Engineers, Bellingham, WA.

Costello, D. K., Carder, K. L. and Hou, W. (1994) Some effects of the sensitivity threshold and spatial resolution of a particle imaging system on the shape of the measured particle size distribution. In *Ocean Optics XII, Proceedings of the SPIE 2258*, ed. J. S. Jaffe, pp. 768–783. Society of Photo-optical Instrumentation Engineers, Bellingham, WA.

Costello, D. K., Carder, K. L. and Hou, W. (1995) Aggregation of diatom bloom in a mesocosm: bulk and individual particle optical measurements. *Deep-Sea Research II*, **42**, 29–45.

Dam, H. G. and Drapeau, D. T. (1995) Coagulation efficiency, organic-matter glues and the dynamics of particles during a phytoplankton bloom in a mesocosm study. *Deep-Sea Research II*, **42**, 111–123.

Dilling, L., Wilson, J., Steinberg, D. and Alldredge, A. L. (1998) Feeding by the euphausiid, *Euphausia pacifical*, and the copepod, *Calanus pacificus*, on marine snow. *Marine Ecology Progress Series*, in press.

Eckhoff, R. K. (1969) A static investigation of the Coulter principle of particle sizing. *Journal of Scientific Instruments*, **2**, 973–977.

Eisma, D. (1986) Flocculation and de-flocculation of suspended matter in estuaries. *Netherlands Journal of Sea Research*, **20**, 183–199.

Friedlander, S. K. (1977) *Smoke, Dust, and Haze*. Wiley, New York.

Graham, W. M. (1993) Spatio-temporal scale assessment of an "upwelling shadow" in northern Monterey Bay, California. *Estuaries*, **16**, 83–91.

Hunt, J. R. (1980a) Prediction of oceanic particle size distributions from coagulation and sedimentation mechanisms. In *Particulates in Water*, eds M. C. Kavanaugh and J. O. Leckie, pp. 243–257. American Chemical Society, Washington, DC.

Hunt, J. R. (1980b) Coagulation in continuous particle size distributions: theory and experimental verification. Ph.D. Thesis, California Institute of Technology, Pasadena.

Hunt, J. R. (1982) Particle dynamics in seawater: implication for predicting the fate of discharged particles. *Environmental Science and Technology*, **16**, 303–309.

Jackson, G. A. (1995) Comparing observed changes in particle size spectra with those predicted using coagulation theory. *Deep-Sea Research II*, **42**, 159–184.

Jackson, G. A. and Lochmann, S. E. (1993) Modeling coagulation of algae in marine ecosystems. In *Environmental Particles, Vol. 2*, eds J. Buffle and H. P. van Leeuwen, pp. 387–414. Lewis, Boca Raton, FL.

Jackson, G. A., Logan, B. E., Alldredge, A. L. and Dam, H. G. (1995) Combining particle size spectra from a mesocosm experiment measured using photographic and aperture impedance (Coulter and Elzone) techniques. *Deep-Sea Research II*, **42**, 139–157.

Jiang, Q. and Logan, B. E. (1996) Fractal dimensions of aggregates from shear devices. *Journal of the American Water Works Association*, **88**(2), 100–113.

Lal, D. (1977) The oceanic microcosm of particles. *Science*, **198**, 997–1009.

Lampitt, R. S., Wishner, K. F., Turley, C. M. and Angel, M. V. (1993) Marine snow studies in the Northeast Atlantic Ocean: distribution, composition, and role as a food source for migrating plankton. *Marine Biology*, **116**, 689–702.

Li, X. and Logan, B. E. (1995) Size distributions and fractal properties of particles during a simulated phytoplankton bloom in a mesocosm. *Deep-Sea Research II*, **42**, 125–138.

Li, X., Passow, U. and Logan, B. E. (1997) Size distributions and fractal dimensions of small (15 to 200 μm) particles from eastern Pacific coastal waters. *Deep-Sea Research I*, in press.

Lines, R. W. (1992) The electrical sensing zone method (the Coulter principle). In *Particle Size Analysis*, eds N. G. Stanley-Wood and R. W. Lines, pp. 350–373. Royal Society of Chemistry, Cambridge.

Lloyd, P. J. (1982) Response of the electrical sensing zone method to non-spherical particles. In *Particle Size Analysis 1981*, eds N. G. Stanley-Wood and T. Allen, pp. 199–208. Wiley Heyden, London.

Logan, B. E. and Kilps, J. R. (1995) Fractal dimensions of aggregates formed in different fluid mechanical environments. *Water Research*, **29**, 443–453.

Logan, B. E. and Wilkinson, D. B. (1990) Fractal geometry of marine snow and other biological aggregates. *Limnology and Oceanography*, **35**, 130–136.

MacIntyre, S., Alldredge, A. L. and Gotschalk, C. C. (1995) Accumulation of marine snow at density discontinuities in the water column. *Limnology and Oceanography*, **40**, 449–468.

Maffione, R. A., Dana, D. R., Voss, J. M. and Frysinger, G. S. (1993) Instrumented remotely operated vehicle for measuring inherent and apparent optical properties of the ocean, In *Underwater Light Measurements, Proceedings of the SPIE 2048*, ed. H. C. Eilertsen, pp. 124–137. Society of Photo-optical Instrumentation Engineers, Bellingham, WA.

McCave, I. N. (1983) Particulate size spectra, behavior, and origin of nepheloid layers over the Nova Scotian continental rise. *Journal of Geophysical Research*, **88**, 7647–7666.

McCave, I. N. (1984) Size spectra and aggregation of suspended particles in the deep ocean. *Deep-Sea Research*, **31**, 329–352.

McCave, I. N. (1985) Properties of suspended sediment over the HEBBLE area on Nova Scotian rise. *Marine Geology*, **66**, 169–188.

Risović, D. and Martinis, M. (1996) Fractal dimensions of suspended particles in seawater. *Journal of Colloid and Interface Science*, **182**, 199–203.

Rodriquez, J. and Mullin, M. M. (1986) Diel and interannual variation of size distribution of oceanic zooplankton biomass. *Ecology*, **67**, 215–222.

Rogak, S. N. and Flagan, R. C. (1990) Stokes drag on self-similar clusters of spheres. *Journal of Colloid and Interface Science*, **134**, 206–218.

Shanks, A. and Waters, K. (1996) Feeding by a heterotrophic dinoflagellate (*Noctiluca scintillans*) in marine snow. *Limnology and Oceanography*, **41**, 177–181.

Sheldon, R. W. and Kerr, S. R. (1972) The population density of monsters in Loch Ness. *Limnology and Oceanography*, **17**, 796–798.

Sheldon, R. W., Prakash, A. and Sutcliffe, W. H. (1972) The size distribution of particles in the ocean. *Limnology and Oceanography*, **17**, 327–340.

Smayda, T. R. (1970) The suspension and sinking of phytoplankton in the sea. *Oceanography and Marine Biology Annual Review*, **8**, 353–414.

Smith, D. C., Simon, M., Alldredge, A. L. and Azam, F. (1992) Intense hydrolytic enzyme activity on marine aggregates and implications for rapid particle dissolution. *Nature*, **359**, 139–142.

Sternberg, R. W., Kranck, K., Cacchione, D. A. and Drake, D. E. (1988) Suspended sediment transport under estuarine tidal channel conditions. *Sedimentary Geology*, **57**, 257–272.

Strathmann, R. R. (1977) Estimating the organic carbon content of phytoplankton from cell volume or plasma volume. *Limnology and Oceanography*, **12**, 411–418.

Trent, J. D., Shanks, A. L. and Silver, M. W. (1978) *In situ* and laboratory measurements on macroscopic aggregates in Monterey Bay, California. *Limnology and Oceanography*, **23**, 626–635.

Treweek, G. P. and Morgan, J. J. (1977) Size distribution of flocculated particles: application of electronic particle counters. *Environmental Science and Technology*, **11**, 707–714.

Van der Plaats, G. and Herps, H. (1984) A study of the sizing process of an instrument based on the electrical sensing zone principle. Part 2. The influence of particle porosity. *Powder Technology*, **38**, 73–76.

Vicsek, T. (1992) *Fractal Growth Phenomena*, 2nd edn. World Scientific, Singapore, 488 pp.

APPENDIX

Relationship between particle size spectra

The relationship between particle spectra for size expressed as conserved diameter d_c and image diameter d_I can be described using fractal scaling as

$$d_c = \lambda_I^{D/3} \tag{A1}$$

where $\lambda = d_0^{1-D/3}$ and d_0 is the monomer diameter.

For a particle size spectrum that is linear in a log–log plot,

$$n_c = a d_c^{-b} \tag{A2}$$

where n_c is the particle size spectrum of particles for the conserved diameter and a and b are constants.

The particle size spectrum for d_I can be calculated as

$$\begin{aligned} n_I &= n_c \frac{dd_c}{dd_I} \\ &= \frac{aD}{3} \lambda^{1-b} d_I^{[(D/3)-(Db/3)-1]}. \end{aligned} \tag{A3}$$

If n_I is plotted as a function of d_I on the same plot that n_c is plotted as a function of d_c, then the two lines intersect when $d_c = d_I = d_x$ and $n_c = n_I$. Setting $n_c = n_I$ and solving for d_x yields

$$d_x = \gamma d_0 \tag{A4}$$

where

$$\gamma = (3D)^{\frac{1}{[1-(D/3)](b-1)}}.$$

The relative size of γ can be seen by calculating it for a range of values of D and b: $D = 1.5$, $b = 4$, $\gamma = 1.59$; $D = 2.5$, $b = 4$, $\gamma = 1.44$; $D = 2.5$, $b = 3$, $\gamma = 1.73$; $D = 1.5$, $b = 3$, $\gamma = 2$. Thus, for the range of values expected for D and b, the crossover diameter d_x is within a factor of two of the monomer diameter, d_0.